Incorporation of trivalent cations in NaX zeolite nanocrystals for the adsorption of O 2 in the presence of CO 2

Sarah Komaty, Ayoub Daouli, Michael Badawi, Clément Anfray, Moussa Zaarour, Valable Samuel, Svetlana Mintova

▶ **To cite this version:**

ARTICLE

Incorporation of trivalent cations in NaX zeolite nanocrystals for the adsorption of O₂ in the presence of CO₂

Sarah Komaty,[a] Ayoub Daouli,[b] Michael Badawi,[b] Clément Anfray,[c] Moussa Zaarour,[a] Samuel Valable,[c] Svetlana Mintova[*a]

The O_2 and CO_2 sorption properties of nanosized zeolite X with faujasite type structure through a partial ionic exchange of sodium (Na^+) by trivalent cations (Gd^{3+} and Ce^{3+}) were evaluated. Three faujasite samples were studied, the as-synthesized Na-X possessing Na^+ solely, and the modified samples Na-Gd-X and Na-Ce-X containing Gd^{3+} (1.8 wt%) and Ce^{3+} (0.82 wt%), respectively. Incorporating scarce amounts of trivalent cations modified the adsorption affinity of zeolites towards O_2 and CO_2 as demonstrated by *in situ* Fourier-transform infrared spectroscopy (FTIR). While Na-Ce-X encounters the highest O_2 physisorption capacity, the Na-Gd-X is adsorbing the highest quantities of molecular CO_2. All three samples exhibit the chemisorbed CO_2 in the form of carbonates, while the Na-X stores carbonates in monodentate and polydentate forms, the Na-Gd-X and Na-Ce-X allow the formation of polydentate carbonates only. Density functional theory (DFT) calculations revealed that trivalent cations tend to adsorb gases through two cations simultaneously which explains the presence of polydentate carbonates exclusively in the corresponding modified zeolites. The DFT results confirmed the higher affinity of Na-Gd-X and Na-Ce-X nanocrystals towards O_2 in the presence of CO_2. The affinity of Na-Gd-X and Na-Ce-X nanocrystals towards O_2 opens the door of their use as oxygen transporters for medical applications where CO_2 is constantly present. The toxicity of the nanosized zeolites and their performance in O_2 release are reported too.

Introduction

Zeolites are crystalline materials with well-defined framework structures consisting of pores and cages of different sizes and shapes. The large micropore volume, high external surface area[1] and the exchangeable charge compensating cations are fascinating features of zeolites. The systematic control of these parameters allows a facile modulation of the physical and chemical properties of zeolites to tailor them towards target applications, such as selective gas sensors, separation membranes, medical applications, hosts for guest molecules, and even gas carriers.[2,3]

Faujasite type zeolite (zeolite X) is widely used in the adsorption and the separation processes owing to the large free volume available to accommodate desired gases and various metal cations.[4] Additionally, template free zeolites have shown non-toxic behaviour thus promoting the interest in their use for biological and biomedical applications[5,6] such as the storage and transportation of respiratory gases including carbon dioxide and dioxygen.[7,8] We have recently reported on the synthesis and sorption properties of faujasite zeolite nanocrystals.[6,9]

Herein, we report experimental results and theoretical DFT calculations on the impact of trivalent cations in the faujasite zeolite nanocrystals on their sorption capacities for O_2 and CO_2. The as-synthesized sodium form of faujasite zeolite (sample Na-X) is used as a reference and compared with samples containing trivalent metal cations Ce^{3+} (sample Na-Ce-X) and Gd^{3+} (sample Na-Gd-X). We have already shown that cerium (Ce^{3+}) can improve the oxygen loading capacity of the zeolites.[6] Therefore cerium and gadolinium were selected to be introduced in the zeolite nanocrystals; such properties of Ce- and Gd- containing zeolites will allow localizing the nanocrystals in the tissues and reveal the regions of action as well as the regions of their accumulation after releasing the O_2. The crystallinity, composition, stability, and textural properties of the as-synthesized and ion-exchanged faujasite samples were characterized by various means including X-ray diffraction (XRD), thermogravimetric analysis (TG), dynamic light scattering and zeta potential (DLS), inductive coupled plasma (ICP), and N_2 sorption analyses. Furthermore, the adsorption behaviour of zeolite nanocrystals toward oxygen and carbon dioxide was evaluated using *in situ* FTIR spectroscopy. Our data revealed the high sorption capability and reversible adsorption/desorption of respiratory gases (CO_2

a. *Normandie Univ., UNICAEN, CNRS, ENSICAEN, Laboratoire Catalyse et Spectrochimie (LCS), 14050 Caen, France.*

b. *Laboratoire de Physique et Chimie Théoriques UMR 7019 CNRS-Université de Lorraine, Nancy, France.*

c. *Normandie Univ, UNICAEN, CEA, CNRS, ISTCT/CERVOxy group, GIP Cyceron, Caen, France.*

and O_2) of nanosized zeolites; the quantity of loaded gases being controlled by the charge compensating cations, thus generating selective gas storage and controlled delivery. The selective adsorption of O_2 in the presence of CO_2 is very challenging, as most of zeolites will adsorb preferably CO_2.[10–14] The experimental results were supported by DFT calculations, which in turn highlight that the adsorption selectivity of O_2 towards CO_2 may be largely enhanced if Ce^{3+} cations pairs are embedded in the nanosized zeolites.

Experimental part

Preparation of nanosized faujasite zeolite

The as-synthesized nanosized faujasite zeolite, Na-X (particle size of 10 - 20 nm) with Si /Al = 1.32, was prepared following the originally reported procedure by our group.[15] The zeolite nanocrystals were purified by centrifugation and then subjected to freeze drying prior further characterization. No calcination of the samples was carried out due to the absence of organic template.

Ion exchange of nanosized faujasite zeolite

The as-synthesized zeolite (Na-X) was ion-exchanged with gadolinium (III) nitrate hexahydrate $Gd(NO_3)_3.6H_2O$ (sample Na-Gd-X) and cerium (III) chloride pentahydrate $CeCl_3.5H_2O$ (sample Na-Ce-X).

25 mL of $Gd(NO_3)_3.6H_2O$ (3 mM) or $CeCl_3.5H_2O$ (3 mM) were added in 5 ml of Na-X suspensions (2.5 %). The suspensions were then kept under stirring at room temperature for 1 h and then washed by double distilled water. This procedure was performed once to obtain sample Na-Gd-X and repeated twice to obtain sample Na-Ce-X.

Characterization

Dynamic light scattering (DLS) and zeta potential

The size of the nanoparticles was measured by a Malvern Zetasizer Nano instrument using a backscattering geometry (scattering angle of 173°, He–Ne laser with a 3 mW output power at a wavelength of 632.8 nm). The DLS analyses were performed on samples with a solid concentration of 1 wt %. The surface charge of the crystals was determined by measuring the zeta potential value of zeolite nanocrystals in water suspensions at a constant solid concentration (1 wt %) and pH = 8.5.

X-ray diffraction (XRD)

The crystallinity of the zeolite powder samples (Na-X, Na-Gd-X and Na-Ce-X) was studied by XRD; the XRD patterns were recorded by a *PANalytical* X'Pert Pro diffractometer with CuK α monochromatized radiation (λ = 1.5418 Å).

Inductively coupled plasma (ICP)

The chemical composition of the zeolites was determined by inductively coupled plasma optical emission spectroscopy using a Varian ICP-OES 720-ES.

N₂ sorption analysis

The porosity of the samples was measured using a Micrometrics ASAP 2020 volumetric adsorption analyzer. Samples were degassed at 275 °C under vacuum overnight before the measurement. The external surface area and micropore volume were estimated by the alpha-plot method using Silica-1000 (22.1 m^2 g^{-1} assumed) as a reference. The micropore and mesopore size distributions of solids were estimated by the Nonlocal Density Functional Theory (NLDFT) and Barret-Joyner-Halenda (BJH) method using the desorption branch, respectively.

Thermogravimetric analysis (TGA)

The water content and stability of the samples were investigated using a SETSYS instrument (SETARAM) analyzer (heating rate of 5 °C min^{-1} under 40 $ml.min^{-1}$ flow of air).

In situ FTIR spectroscopy

Powder zeolite samples (Na-X, Na-Gd-X and Na-Ce-X) were pressed (~10^7 Pa) into self-supported disks (2 cm^2 area, 20 $mg.cm^{-2}$). *In situ* IR spectra were recorded using a Nicolet 6700 IR spectrometer (ThermoScientific, Villebon sur Yvette, France) equipped with a mercury cadmium telluride (MCT) detector and an extended KBr beam splitter. Spectra were recorded in the 400-5500 cm^{-1} range at 4 cm^{-1} with 128 scans. A homemade IR cell was used to evacuate the samples, then samples were heated up to 200 °C for 2 h under vacuum prior to the measurements, and cooled down to -196°C. Various amounts of oxygen (0–102 Torr) and carbon dioxide (0-1.5 Torr) were introduced into the cell and kept in equilibrium for 5 min in the case of O_2, and 1 min in the case of CO_2 before recording each spectrum. The zeolites were loaded with increasing amounts of O_2 and CO_2 till their corresponding FTIR bands reached saturation. To allow the comparison of different samples, all spectra were normalized to the samples' mass and plotted as absorbance per gram over the wavelength.

DFT calculations

The adsorption modes and interactions energies of CO_2 and O_2 and cationic-exchanged zeolites have been investigated through density functional theory (DFT). All the calculations were performed using the Vienna Ab initio Simulation Package (VASP),[16] with a planewave basis set and projector augmented wave (PAW) pseudopotentials.[17] The PBE functional[18] was used combined with the D2 correction to account for dispersion forces.[19,20] The plane wave cutoff energy was set to 500 eV, and the Brillouin zone sampling at the Γ-point. The Kohn-Sham equations were solved self-consistently until energy difference between cycles become lower than 10^{-6} eV, and the atomic positions have been fully optimized until all forces were smaller than 0.03 eV/ Å per atom. For open-shell cations, the DFT+U method of Hubbard[21] was used with U = 6.7 and 5 eV for cerium and gadolinium, respectively.[22] Previous work has also shown that the correct localization of excess electrons on Ce ions is only achieved for U = 5 eV and higher.[23]

In the present study, we use a primitive rhombohedral cell of FAU containing around 165 atoms to reduce computational effort.[24–27] It can be seen in Figure 1 that the primitive cell of faujasite contains two supercages and eight hexagonal windows connecting the sodalite with the supercage.[25,28]
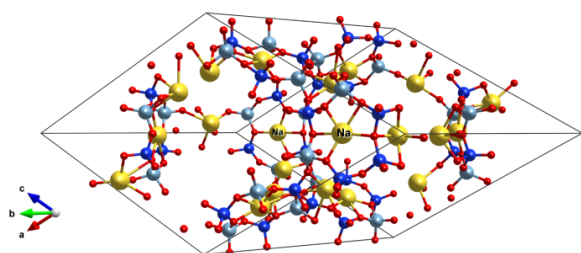
Figure 1. Periodic model used for faujasite sample Na-X (Si/Al=1.28): primitive cell, 165 atoms (21 Na, 21 Al, 27 Si, 96 O).

Interaction energies have been calculated according to the following equation:

$$\Delta E_{int} = E_{FAU-M} - (E_{FAU} + E_M)$$

Where ΔE_{int} is the adsorption energy, E_{FAU+M} is the total energy of the zeolite with the adsorbate, and E_{FAU} and E_M are the total energies of isolated adsorbate and bare zeolite, respectively.

Cell lines

A human glioblastoma cell line, U87-MG purchased from American Type Culture Collections (ATCC, Manassas, VA, USA) was used. Cells were cultured in Dulbecco's Modified Eagle Medium (DMEM, Sigma-Aldrich, France). DMEM was supplemented with 10 % fetal bovine serum (Eurobio, France), 2 mM glutamine (Sigma-Aldrich, France) and 100 U/ml penicillin/streptomycin (Sigma-Aldrich, France). Cells were maintained in culture at 37 °C with 5 % CO_2 and 95 % humidity.

Primary culture of astrocytes

Cerebral cortices were isolated from neonatal (1 to 3-day-old) mice (Swiss, CURB, France) carefully stripped of the meninges and dissociated to generate a single-cell suspension. Cultures were allowed to grow in a humidified 5 % CO_2 incubator at 37 °C to confluency (15-20 days) prior to use in DMEM supplemented with 10 % foetal bovine serum (Eurobio, France), 10 % horse serum (Eurobio, France), 2 mM glutamine (Sigma-Aldrich, France) and 100 U/ml penicillin/streptomycin (Sigma-Aldrich, France). At about 80 % confluence, the growth medium was replaced by the same medium.

Cells exposure to nanosized zeolites

Cells were exposed to nanosized zeolites (Na-X, Na-Ce-X, and Na-Gd-X) up to 48 h. Zeolites were diluted in culture medium at a concentration of 50, 100 or 400 µg/ml and added directly into the wells. Control tests (distilled water) in the wells with the same volumes were performed.

Cell viability

The concentration range to test was determined using the following assumption: the average blood volume of a rat is ~64 mL/kg. Given that 250-300 mg animals were used in the in vivo experiments, the rats had 16-19 ml of blood. 300 µl of a 1 wt %. solution, which is 3 mg of material, equates to a maximum of ~156-188 µg zeolite/mL of blood.

Cells were seeded in 24-wells plates to achieve 80 % confluency for the control on the day of the analysis. Cell viability was assessed 48 h following the exposure to zeolites

with the WST-1 assay (Roche, France) according to the manufacturer's instructions.

Release of oxygen in aqueous and hypoxic conditions

A hypoxia workstation (IN VIVO2 500, 3M) was used to obtain a stable and controlled gas composition of the atmosphere with a precision of 0.1 % O_2 by adapting the amount of N_2. Phosphate buffered saline (PBS, Sigma-Aldrich) solution was equilibrated in the hypoxia chamber for 1 h prior to the experiment. A closed reaction vessel containing 12 ml of equilibrated PBS at 37 °C, and a dissolved oxygen sensor (SevenGo (Duo) pro™ / OptiOx™, Mettler Toledo) was used inside the hypoxia chamber. Prior to the experiments, the baseline was established by measuring the oxygen saturation in the system for 30 min. Nanosized zeolites (Na-X, Na-Gd-X, and Na-Ce-X) were then added to the system, and the oxygen dissolved in the PBS solution was measured continuously for 1h. The oxygen release capacity of nanosized zeolites (Na-X, Na-Gd-X and Na-Ce-X) was compared to the baseline situation and expressed as a change relative to baseline.

Statistical analyses. Data are presented as mean ± s.d. HSD Tuckey post-hoc test using a two-way ANOVA with the JMP programs (SAS Institute)

Results and Discussion

XRD patterns reflecting the crystallinity and purity of phases with Bragg peaks typical of faujasite zeolite structure were recorded for the as-synthesized (Na-X), the cerium (Na-Ce-X), and the gadolinium (Na-Gd-X) ion-exchanged zeolite samples (Figure 2). The crystallinity of the as-synthesized Na-X zeolite is highly preserved throughout the ion-exchange process.
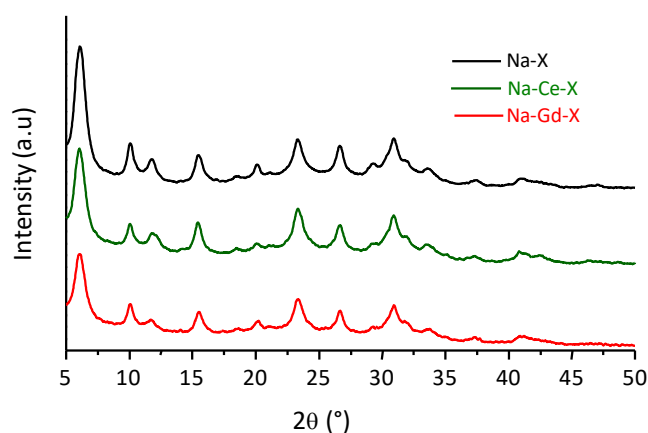

Figure 2. XRD patterns of the as-synthesized (Na-X), gadolinium ion-exchanged (Na-Gd-X) and cerium ion-exchanged (Na-Ce-X) zeolite samples.

The as-synthesized and ion exchange samples contain discrete nanoparticles of 10-20 nm with narrow and monomodal particle size distribution (Figure S1). These nanocrystals are highly stable in water suspension which is confirmed by the measured zeta potential values of -39 mV (Na-Gd-X) to -43 mV (Na-Ce-X) (Figure S2). Besides, the partial replacement of Na^+ by Ce^{3+} or Gd^{3+} does not seem to affect the crystallinity of the zeolites; the Si/Al ratio is almost constant for all samples, as shown by ICP (Table 1).

The TG curves contain peaks that correspond to the removal of water molecules solely (Figure 3). For instance, a main mass loss was detected at 85 °C in the case of Na-X and Na-Ce-X samples corresponding to the removal of the physisorbed water. A second important loss was identified at 135 °C (Na-X) or at 119 °C (Na-Ce-X) which is linked to the water molecules adsorbed in the channels of the zeolite that is strongly related with the presence of cations. A different behaviour was recorded for Na-Gd-X with
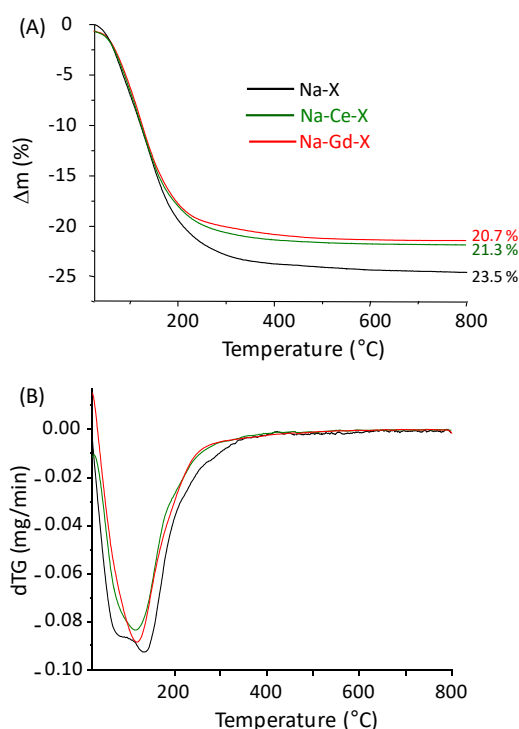

Figure 3. (A) Thermogravimetric analysis and (B) differential thermogravimetric analysis curves of the as-synthesized (Na-X), gadolinium ion-exchanged (Na-Gd-X) and cerium ion-exchanged (Na-Ce-X) zeolite samples.

one single weight loss at 119 °C (Figure 3). The ion exchange modification of nanosized faujasite samples induced a slight increase in their hydrophobicity, and the water content decreases following the order: Na-X (23.5 % H_2O) > Na-Ce-X (21.3% H_2O) > Na-Gd-X (20.7% H_2O).

Sample	Chemical composition (wt %)				
	Si (wt %)	Al (wt %)	Na (wt %)	*M (wt %)	Si/Al
Na-X	19.9	15.1	11.2	0	1.32
Na-Ce-X	17.6	13.5	11.0	0.82	1.30
Na-Gd-X	17.9	13.8	10.7	1.80	1.30

Table 1. Chemical composition of the as-synthesized Na-X, gadolinium ion-exchanged (Na-Gd-X) and cerium ion-exchanged (Na-Ce-X) zeolite samples.

The chemical formula based on the ICP results for the samples were calculated: Na-X: [$Na_{85}(H_2O)_{228}$ [$Si_{107}Al_{85}O_{384}$], Na-Ce-X: [$Na_{84}Ce_1(H_2O)_{201}$ [$Si_{107}Al_{85}O_{384}$], and Na-Gd-X: [$Na_{79}Gd_2(H_2O)_{188}$ [$Si_{107}Al_{85}O_{384}$].

Nitrogen sorption analyses of sample Na-X revealed Type I isotherm with high N_2 uptake at low partial pressure (P/P0) characteristic for microporous materials, and another high uptake at P/P0 > 0.8 attributed to the high textural mesoporosity resulting from the closely packed zeolite nanoparticles with similar particle sizes (Figure 4). These properties were highly preserved upon the incorporation of the various charge compensating cations. More specifically, the high surface area (760 $m^2.g^{-1}$) and large micropore volume (0.28 $cm^3.g^{-1}$) calculated for Na-X (Table 2) were very close to
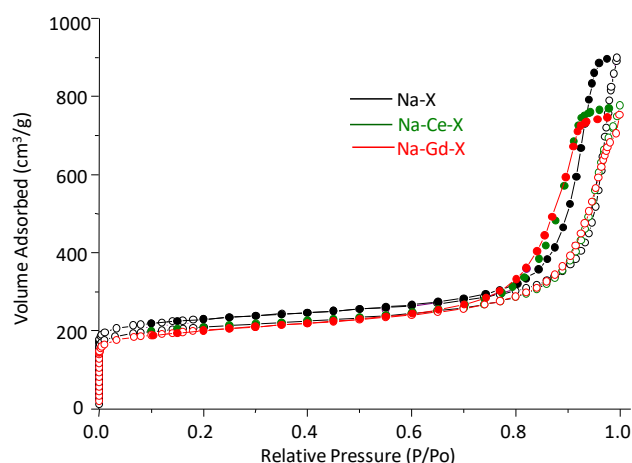
those of Na-Gd-X and Na-Ce-X zeolite samples.

Figure 4. Nitrogen isotherms (full circles: adsorption/ empty circles: desorption) of the as-synthesized (Na-X), gadolinium ion-exchanged (Na-Gd-X) and cerium ion-exchanged (Na-Ce-X) zeolite samples.

Table 2. Surface area and pore volume of the as-synthesized (Na-X), gadolinium ion-exchanged (Na-Gd-X) and cerium ion-exchanged (Na-Ce-X) zeolite samples.

Sample	S_{BET} ($m^2.g^{-1}$)	V_{mic} ($cm^3.g^{-1}$)	V_{total} ($cm^3.g^{-1}$)
Na-X	760	0.28	1.39
Na-Ce-X	753	0.26	1.21
Na-Gd-X	749	0.26	1.18

CO_2 adsorption properties of zeolite nanocrystals

The CO_2-zeolite interaction is known to take place via the zeolite charge compensating cations. The incorporation of alkaline earth or alkali metals on the surface and/or in the voids of zeolite promotes their basic character and increases further the zeolite affinity towards such acidic gas.[29,30] Carbon dioxide can be adsorbed on the zeolite in two different forms (Figure 5): (1) the physisorbed CO_2 where the gas is immobilized in its molecular form following weak interactions with the zeolite, and (2) the chemisorbed CO_2 where it is stored as carbonates chemically bonded to the zeolite. In regards to the limited space available on the surface and channels of the zeolite, the formation of carbonates is expected to reduce the free space available for the adsorption of molecular CO_2. Several additional factors can eventually

affect the zeolite affinity towards the adsorption of carbon dioxide, including the zeolite structure, zeolite hydrophilicity (hence the quantity of available water), the size, the type and the quantity of charge compensating cations.[31,32]
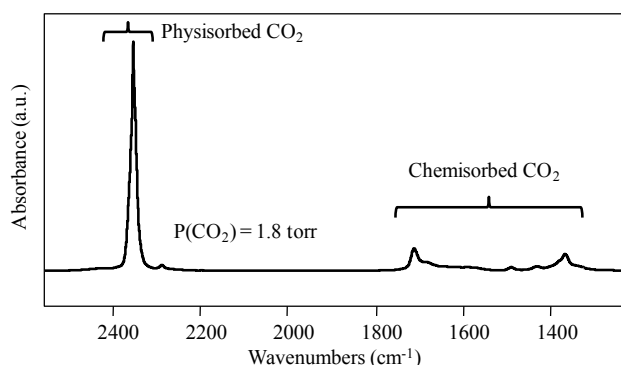

Figure 5. FTIR spectrum of CO_2 adsorbed on as-synthesized Na-X zeolite (25°C).

Experimental results revealed the adsorption of CO_2 in both physisorbed and chemisorbed modes on all zeolite samples (Figure 6). The former appears as an intense band centered at 2354 cm^{-1}, while the different carbonate species are distinguished as a set of bands extending from 1750 cm^{-1} to 1300 cm^{-1}.

The impact of charge compensating cations on the physisorption of CO_2 is illustrated in Figure 7. Incorporating gadolinium (Na-Gd-X) induce an increase of CO_2 loading by 11 % while the cerium (Na-Ce-X) reduced the zeolite affinity towards CO_2 by 15 %.

CO_2 can chemically bind to zeolite in a quasi-irreversible process giving rise to different carbonate species such as mono-, bi-, and polydentate carbonates.[33,34,35] In our case, polydentate carbonates also referred to as "bridged bidentate carbonates" identified by the IR bands at 1710 cm^{-1} and 1364 cm^{-1} [19,36] (Figure 6); the bridged bidentate carbonates were recorded in all three samples with the highest levels for the Na-Gd-X sample. On the other hand, the monodentate species appeared as well; the IR bands at 1485 cm^{-1} and 1430 cm^{-1} with comparable intensities to polydentate appeared only for sample Na-X (Figure 8).[36] Apparently, the monovalent Na^+ favours the formation of monodentate carbonates, whereas trivalent Gd^{3+} and Ce^{3+} cations favour the formation of polydentate species with no traces of monodentate being detected.

O_2 adsorption properties of zeolite nanocrystals

The exposure of the zeolite samples to O_2 pressure generates an IR band at 1554 cm^{-1} (Figure 9). This is clear evidence of the successful adsorption of the symmetrical O_2 molecules on the zeolite, and consequently, the altering of its symmetry that prevents any detectable IR band in its gas phase.[6] Different sites of zeolites are available for the oxygen adsorption including, the Brønsted acid sites, and the charge compensating cations[37] identified by the FTIR bands at 1553 cm^{-1} and 1557 cm^{-1}, respectively. In our case, broadband

extends from 1570 cm^{-1} to 1545 cm^{-1}. Considering that the zeolite samples used in this study are present in the cationic form and not in the H-form, the oxygen is believed to adsorb on the Na^+ for (Na-X), Na^+ and Ce^{3+} for (Na-Ce-X), and Na^+ and Gd^{3+} cations for (Na-Gd-X). Repetitive adsorption/desorption cycles resulted in the reproducible appearance/disappearance of the band at 1554 cm^{-1} with no remarkable decrease in intensity, thus confirming (1) its attribution to O_2 adsorption, and (2) demonstrating the high capability of the zeolite
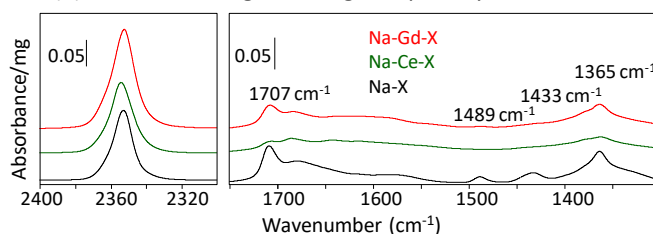
samples for O_2.

Figure 6. Evolution of the IR spectra of the as-synthesized (Na-X), gadolinium ion-exchanged (Na-Gd-X) and cerium ion-exchanged (Na-Ce-X) zeolite samples during the CO_2 adsorption. All spectra were subtracted from the IR spectrum of the corresponding samples after activation at 250°C under vacuum.
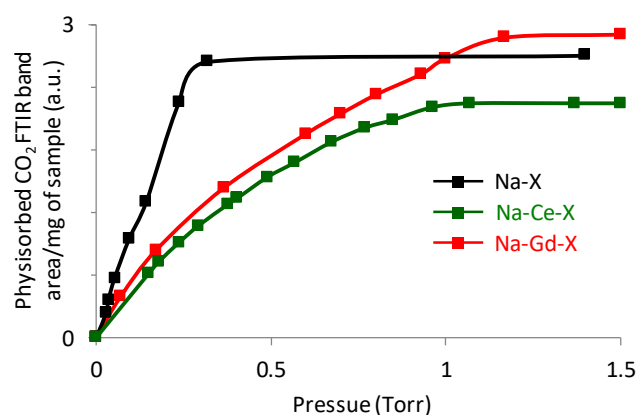

Figure 7. Physisorbed CO_2 FTIR band area normalized to the mass of the as-synthesized (Na-X), gadolinium ion-exchanged (Na-Gd-X) and cerium ion-exchanged (Na-Ce-X) zeolite samples at various CO_2 pressure of 0.1-1.5 Torr.
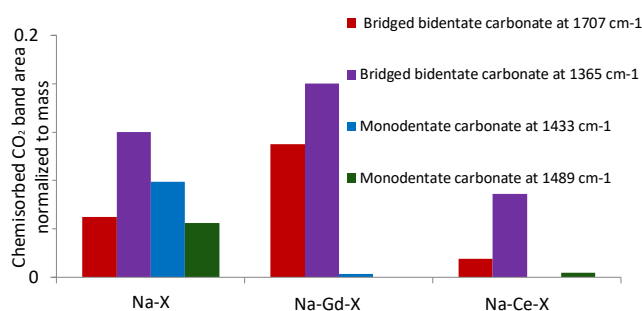

Figure 8. Different carbonate species detected on the as-synthesized (Na-X), gadolinium ion-exchanged (Na-Gd-X) and cerium ion-exchanged (Na-Ce-X) zeolite samples by FTIR.
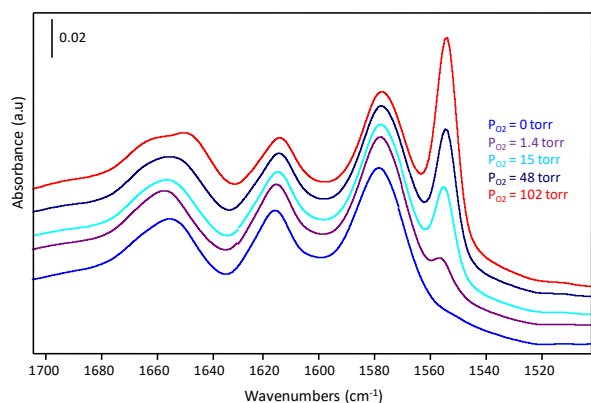
Figure 9. FTIR spectra of as-synthesized Na-X before and after adsorption of various O2 pressures at -196 °C.

The trivalent cations are found to slightly enhance the capacity of zeolite nanocrystals towards O_2 (Figure 10); the affinity towards O_2 increased by 5% and 13% following the incorporation of Gd^{3+} (Na-Gd-X) and Ce^{3+} (Na-Ce-X) in the zeolite samples, respectively. This is ascribed to the fact that introducing one trivalent cation requires the removal of three Na^+ cations, which releases additional volume available to host more molecules. In addition to the higher O_2 loading, the trivalent cations in samples Na-Gd-X and Na-Ce-X promote a faster loading of O_2 as revealed by the higher slope of the curve presenting the area of oxygen versus pressure introduced (Figure 10).
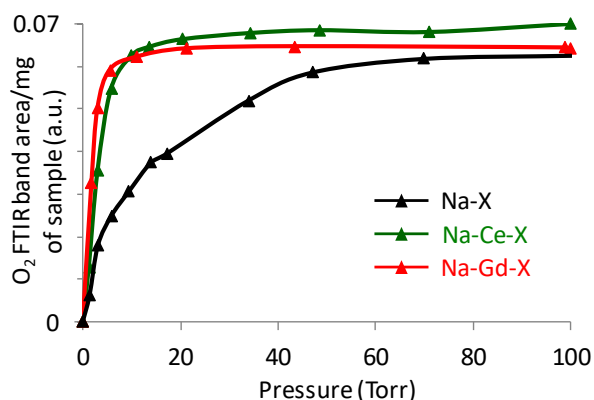

Figure 10. O_2 FTIR band area normalized to the mass of the as-synthesized (Na-X), gadolinium ion-exchanged (Na-Gd-X) and cerium ion-exchanged (Na-Ce-X) zeolite samples as a function of O_2 pressures.

Density functional theory (DFT) calculations

In the first step, DFT calculations were performed for the three zeolite models: Na-Na which contains 21 Na^+ cations for two supercages (Na-X experimental sample); Na-Ce which contains 18 Na^+ cations and one Ce^{3+} cation (Na-Ce-X experimental sample); Na-Gd which contains 18 Na^+ cations and one Gd^{3+} cation (Na-Gd-X experimental sample). We consider isolated trivalent cations surrounded by sodium cations. The two latter models were designed to respect the relative amount of cations measured in the samples by ICP-MS (Table1). The possible O_2 and CO_2 adsorption modes revealed that these gases adsorbed on zeolite via two or three cations simultaneously (Figure 11). Owing to the short distance across

the different charge compensating cations within Na-X, O_2 preferably adsorb by two cations located in the proximity and CO_2 by three cations. Na-X has a stronger affinity for CO_2 rather than O_2 by around 20 kJ/mol (Figure 12). Introducing one trivalent cation (M^{3+}) in the faujasite leads to a change of affinities, provoking the interaction of zeolites with O_2, and the interaction energies of both adsorbed CO_2 and O_2 increase; this enhancement was more pronounced for O_2 (see Figure 7). Higher O_2 adsorption is calculated for the faujasite zeolite nanocrystals containing trivalent cations (Na-Gd-X, Na-Ce-X) in comparison to the as-synthesized Na-X. A similar trend for adsorption of O_2 and CO_2 on the samples was found by *in situ* FTIR study (see Figure 10).

Figure 11. DFT computed adsorption modes of CO_2 in (a) Na-X, (b) Na-Ce-X, and (c) Na-Gd-X , and O_2 in (d) Na-X, (e) Na-Ce-X, and (f) Na-Gd-X samples.
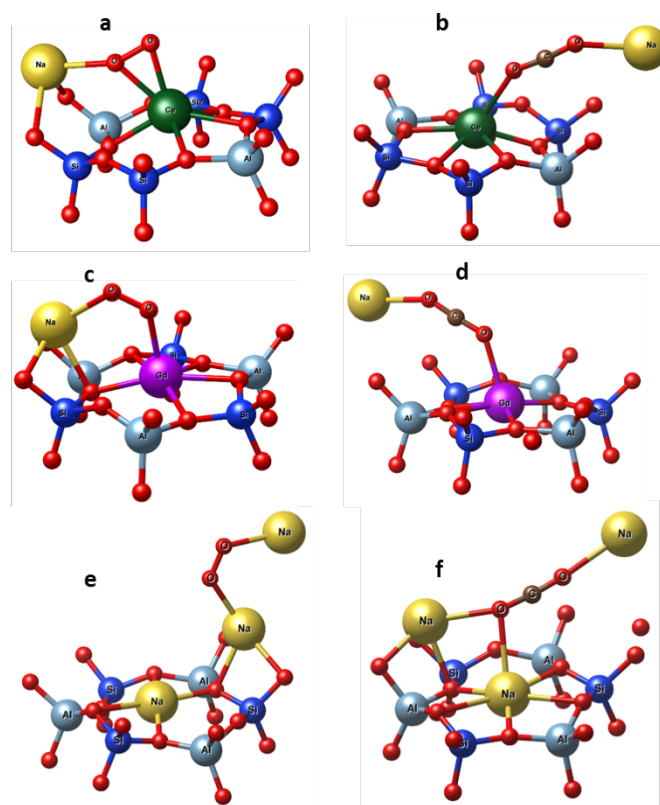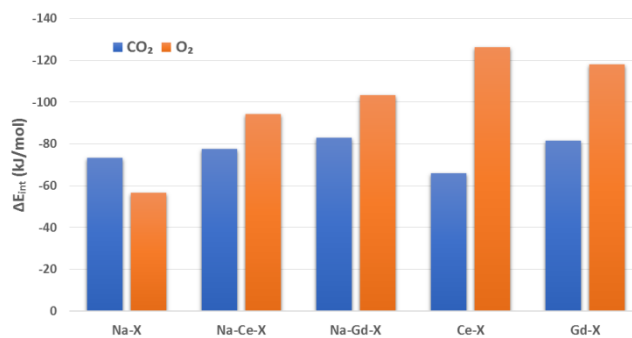

Figure 12. DFT computed interaction energies (ΔE_{int} in kJ/mol) of CO_2 and O_2 on pure Na-X, the partially exchanged faujasite samples with trivalent cations (Na-Ce-X, Na-Gd-X) (corresponding to the experimental samples on this work) and the hypothetic fully exchanged zeolite (Ce-X, Gd-X) samples.

To evaluate the potential of fully exchanged zeolites, we have then considered pure Ce-X and Gd-X models (Figure 13). In contrast to the sample Na-X with a higher affinity towards CO_2 over O_2, the Na-Ce-X and Na-Gd-X zeolites preferably bind to O_2 in the presence of CO_2. This is a highly desirable feature of zeolite nanocrystals for biological applications especially for preferential O_2 delivery where both gases (O_2 and CO_2) are available in the bloodstream. The difference in interaction energy between CO_2 and O_2 over fully exchanged zeolites are very high compared to partially exchanged zeolites (Figure 12). Pure Na-Gd-X zeolite is expected to adsorb O_2 more strongly than CO_2 by 40 kJ/mol, while the pure Na-Ce-X zeolite is expected to adsorb O_2 more strongly than CO_2 by 50 kJ/mol. These results would be further used to motivate the synthesis works to increase the incorporation of trivalent cations in nanozeolites in order to improve their capacity toward O_2.

Figure 13. DFT computed adsorption modes of CO_2 in (a) Ce-X, (b) Gd-X; and O_2 in(c) Ce-X, (d) Gd-X samples.
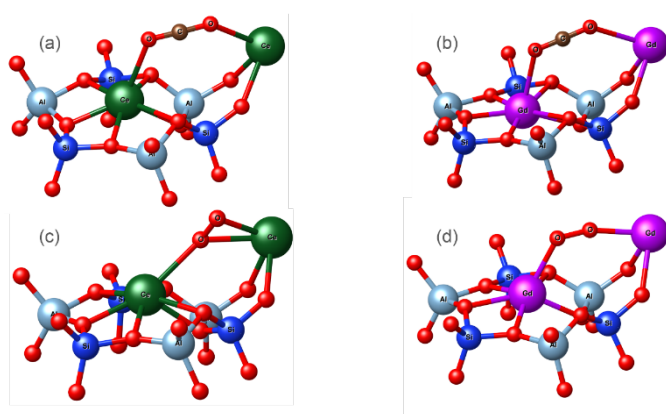
Toxicity of nanosized zeolites

To evaluate further the potential use of nanozeolite for biomedical applications, we performed toxicity measurements on a cell line and a primary cell culture. These cells were exposed to increasing dose of zeolite nanocrystals with either Na-X, Na-Ce-X, and Na-Gd-X zeolite samples. No toxicity was observed on the glioblastoma cell line at all the tested zeolite concentrations (Figure 14).
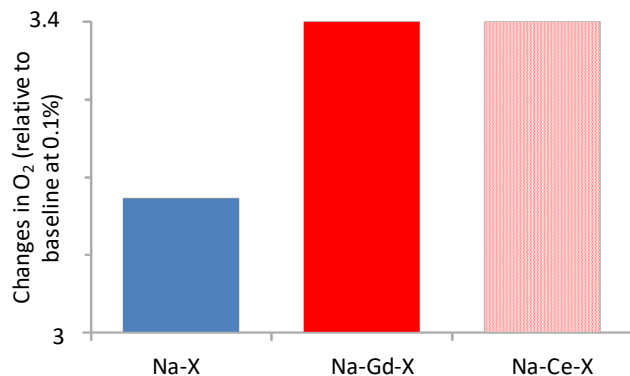

Figure 14. Toxicity measurements of nanosized Na-X, Na-Ce-X, Na-Gd-X zeolites using (a) glioblastoma cell line and (b) primary brain culture for 24 h and 48 h.

For the primary culture, a decrease in cell number was noticed only after 48 h and for the highest dose used (400 µg/ml). Interestingly, no change in the toxicity of the samples was noticed when different cations were introduced in the zeolite samples.

We then measured the ability of zeolite samples to release the oxygen in liquid media. After adding Na-X preloaded with O_2, the changes in oxygen content in the solution measured were 3.17 fold while for Na-Gd-X was 3.4 fold (Figure 15).

Figure 15. Changes in the oxygen content of a PBS solution maintained in hypoxia at 0.2% of O_2 in the workstation following the addition of Na-X or Na-Gd-X zeolites preloaded with O_2. Results are extrapolated for sample Na-Ce-X based
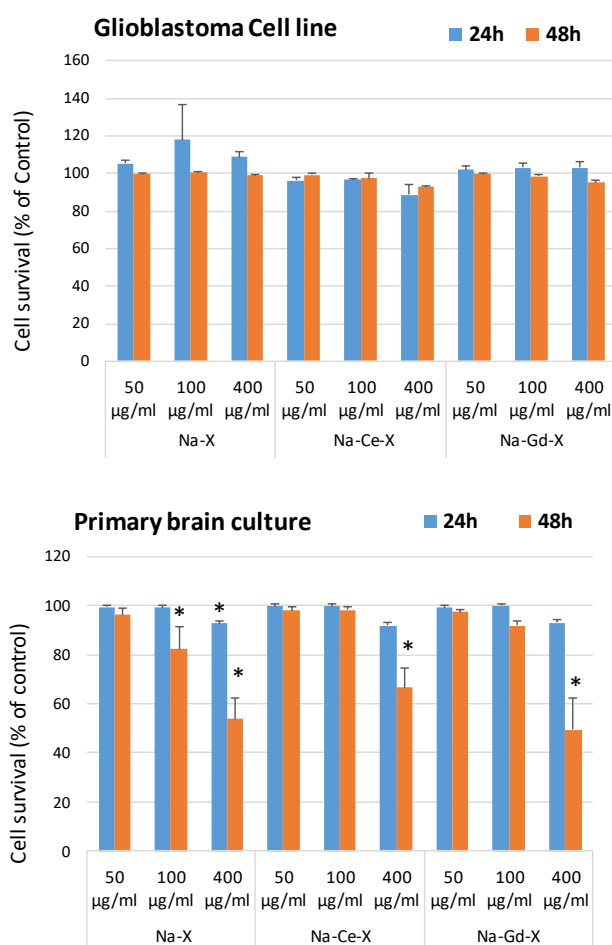
on the results from Figure 10.

Conclusions

The influence of different cations (Na^+, Ce^{3+}, and Gd^{3+}) on the CO_2 and O_2 sorption properties of faujasite zeolite nanocrystals was studied experimentally and by DFT theoretical calculations. The structural and textural properties of the as-synthesized and ion-exchanged zeolite samples were highly preserved. The Na-Gd-X zeolite demonstrated the highest CO_2 physisorption capacity. In contrast, the Na-Ce-X adsorbed 15 % less CO_2 compared to the as-synthesized Na-X zeolite. The incorporated trivalent cations Ce^{3+} and Gd^{3+} favored the

formation of polydentate carbonate over the monodentate one that disappeared completely. These experimental data were validated by theoretical DFT calculations that showed a similar trend toward O_2 and CO_2. Additionally, the easier formation of bi-(poly)dentate carbonates in the presence of trivalent cations (samples Na-Ce-X and Na-Gd-X) is demonstrated. The DFT results show that pure Na-Gd-X zeolite will adsorb O_2 more strongly than CO_2 by 40 kJ/mol, while the pure Na-Ce-X zeolite will adsorb O_2 more strongly than CO_2 by 50 kJ/mol.

Toxicity tests were performed and no toxicity was observed for all three samples using glioblastoma cell line and primary culture; zeolite suspensions with various concentrations were used and the duration of the toxicity test varied from 24 to 48 h. Finally, the potential application of nanosized zeolites with different cations as a transporter for oxygen was demonstrated.

Conflicts of interest

"There are no conflicts to declare".

Acknowledgements

References

1   E. N. Gribov, D. Cocina, G. Spoto, S. Bordiga, G. Ricchiardi and A. Zecchina, *Phys. Chem. Chem. Phys.*, 2006, **8**, 1186–1196.

2   R. E. Morris and P. S. Wheatley, *Angewandte Chemie - International Edition*, 2008, **47**, 4966–4981.

3   D. G. Seifu, T. T. Isimjan and K. Mequanint, *Acta Biomaterialia*, 2011, **7**, 3670–3678.

4   D. M. Ruthven, *Principles of adsorption and adsorption processes.*, John Wiley and Sons, Inc., New York (USA), 1984.

5   S. Laurent, E. P. Ng, C. Thirifays, L. Lakiss, G. M. Goupil, S. Mintova, C. Burtea, E. Oveisi, C. Hébert, M. De Vries, M. M. Motazacker, F. Rezaee and M. Mahmoudi, *Toxicology Research*, 2013, **2**, 270–279.

6   S. Komaty, C. Anfray, M. Zaarour, H. Awala, V. Ruaux, S. Valable and S. Mintova, *Molecules*, , DOI:10.3390/molecules23020037.

7   T. Duke, F. Wandi, M. Jonathan, S. Matai, M. Kaupa, M. Saavu, R. Subhi and D. Peel, *The Lancet*, 2008, **372**, 1328–1333.

8   H. J. Yang, D. Dey, J. Sykes, M. Klein, J. Butler, M. S. Kovacs, O. Sobczyk, B. Sharif, X. Bi, A. Kali, I. Cokic, R. Tang, R. Yumul, A. H. Conte, S. A. Tsaftaris, M. Tighiouart, D. Li, P. J. Slomka, D. S. Berman, F. S. Prato, J. A. Fisher and R. Dharmakumar, *Journal of Nuclear Medicine*, 2017, **58**, 953–960.

9   M. Polisi, J. Grand, R. Arletti, N. Barrier, S. Komaty, M. Zaarour, S. Mintova and G. Vezzalini, *Journal of Physical Chemistry C*, 2019, **123**, 2361–2369.

10 J. A. Dunne, M. Rao, S. Sircar, R. J. Gorte and A. L. Myers, *Langmuir*, 1996, **12**, 5896–5904.

11 R. V. Siriwardane, M.-S. Shen and E. P. Fisher, *Energy Fuels*, 2003, **17**, 571–576.

12 P. Li and F. Handan Tezel, *Microporous and Mesoporous Materials*, 2007, **98**, 94–101.

13 J. Perez-Carbajo, I. Matito-Martos, S. R. G. Balestra, M. N. Tsampas, M. C. M. van de Sanden, J. A. Delgado, V. I. Águeda, P. J. Merkling and S. Calero, *ACS Appl. Mater. Interfaces*, 2018, **10**, 20512–20520.

14 D. Rocca, A. Dixit, M. Badawi, S. Lebègue, T. Gould and T. Bučko, *Phys. Rev. Materials*, 2019, **3**, 040801.

15 H. Awala, J. P. Gilson, R. Retoux, P. Boullay, J. M. Goupil, V. Valtchev and S. Mintova, *Nature Materials*, 2015, **14**, 447–451.

16 G. Kresse and J. Hafner, *Physical Review B*, 1993, **47**, 558–561.

17 D. Joubert, *Physical Review B - Condensed Matter and Materials Physics*, 1999, **59**, 1758–1775.

18 J. P. Perdew, K. Burke and M. Ernzerhof, *Physical Review Letters*, 1996, **77**, 3865–3868.

19 S. Grimme, *Journal of Computational Chemistry*, 2006, **27**, 1787–1799.

20 T. Bučko, J. Hafner, S. Lebègue and J. G. Ángyán, *The Journal of Physical Chemistry A*, 2010, **114**, 11814–11824.

21 A. I. Liechtenstein, V. I. Anisimov and J. Zaanen, *Phys. Rev. B*, 1995, **52**, R5467--R5470.

22 M. Capdevila-Cortada, Z. Łodziana and N. López, *ACS Catalysis*, 2016, **6**, 8370–8379.

23 M. Nolan, S. Grigoleit, D. C. Sayle, S. C. Parker and G. W. Watson, *Surface Science*, 2005, **576**, 217–229.

24 E. P. Hessou, W. G. Kanhounnon, D. Rocca, H. Monnier, C. Vallières, S. Lebègue and M. Badawi, *Theoretical Chemistry Accounts*, 2018, **137**, 161.

25 E. P. Hessou, H. Jabraoui, M. T. A. K. Hounguè, J. B. Mensah, M. Pastore and M. Badawi, *Zeitschrift fur Kristallographie - Crystalline Materials*, 2019, **234**, 469–482.

26 E. P. Hessou, M. Ponce-Vargas, J.-B. Mensah, F. Tielens, J. C. Santos and M. Badawi, *Nanomaterials*, 2019, **9**, 715.

27 J. M. Salazar, M. Badawi, B. Radola, M. Macaud and J. M. Simon, *J. Phys. Chem. C*, 2019, **123**, 23455–23463.

28 M. Chebbi, S. Chibani, J.-F. Paul, L. Cantrel and M. Badawi, *Microporous and Mesoporous Materials*, 2017, **239**, 111–122.

29 J. Zhang, R. Singh and P. A. Webley, *Microporous and Mesoporous Materials*, 2008, **111**, 478–487.

30 I. Hinkov, F. D. Lamari, P. Langlois, M. Dicko, C. Chilev and I. Pentchev, *Journal of Chemical Technology and Metallurgy*, 2016, **51**, 609–626.

31 E. J. Doskocil and R. J. Davis, *Journal of Catalysis*, 1999, **188**, 353–364.

32 J. C. M. Pires, F. G. Martins, M. C. M. Alvim-Ferraz and M. Simões, *Chemical Engineering Research and Design*, 2011, **89**, 1446–1460.

33 E. Gallei and G. Stumpf, *Journal of Colloid And Interface Science*, 1976, **55**, 415–420.

34 R. W. Stevens, R. V. Siriwardane and J. Logan, *Energy and Fuels*, 2008, **22**, 3070–3079.

35 G. Busca and V. Lorenzelli, *Materials Chemistry*, 1982, **7**, 89–126.

36 S. K. Wirawan and D. Creaser, *Microporous and Mesoporous Materials*, 2006, **91**, 196–205.

37 A. B. Ene, M. Bauer, T. Archipov and E. Roduner, *Physical Chemistry Chemical Physics*, 2010, **12**, 6520–6531.